GUT MICROBES
2025, VOL. 17, NO. 1, 2473511
https://doi.org/10.1080/19490976.2025.2473511

Taylor & Francis
Taylor & Francis Group

RESEARCH PAPER

OPEN ACCESS Check for updates

Alcaligenes faecalis promotes colitis to colorectal cancer transition through IgA+ B cell suppression and vinculin acetylation

Jing Zheng[a], Chishun Zhou[a], Zizheng Li[a], Xin Jin[b], Yihua Zou[a], Shasha Bai[a], Huanjin Zheng[a], Weichao Ling[a], Yiru Zhao[a], Ying Wang[a], Rong Zhang[a*], Zhongqiu Liu[a*], and Linlin Lu[a*]

[a]Guangdong Provincial Key Laboratory of Translational Cancer Research of Chinese Medicines, Joint International Research Laboratory of Translational Cancer Research of Chinese Medicines, International Institute for Translational Chinese Medicine, School of Pharmaceutical Sciences, State Key Laboratory of Traditional Chinese Medicine Syndrome, State Key Laboratory of Dampness Syndrome of Chinese Medicine, Guangzhou University of Chinese Medicine, Guangzhou, China; [b]Department of Colorectal Surgery, The First Affiliated Hospital of Guangzhou University of Chinese Medicine, Guangzhou, China

ABSTRACT

Lymphoid tissue-resident commensal bacteria (LRC), a subtype of gut microbiota essential for inflammation-associated carcinogenesis, predominantly attribute to colorectal cancer(CRC), whereas its role was largely unknown. Herein, we found *Alcaligenes faecalis* (*A. faecalis*), the main LRC embedded in Peyer's patches, was abundantly enriched in colitis, adenoma, and stage-dependently observed in CRC tissues. Interestingly, *A. faecalis* alone can not affect intestinal homeostasis, while during colitis, *A. faecalis* significantly translocated from Peyer's patches to colon, remarkably attenuated immune response abilities of B cells, T cells, and DC cells in PPs, consequently impeded IgA+ B cells homing. Meanwhile, during colitis, the ectopia of *A. faecalis* in colon tissues, promoted vinculin acetylation by *A. faecalis*–derived metabolite acetic acid, which impeded intestinal barrier via hindering the binding of vinculin to β-catenin. Our study revealed *A. faecalis* not only suppress mucosal immune responses via reducing IgA+ B cells in Peyer's patches but also disrupt intestinal barrier via increasing vinculin acetylation, ultimately promoting inflammation-to-cancer transition in CRC.

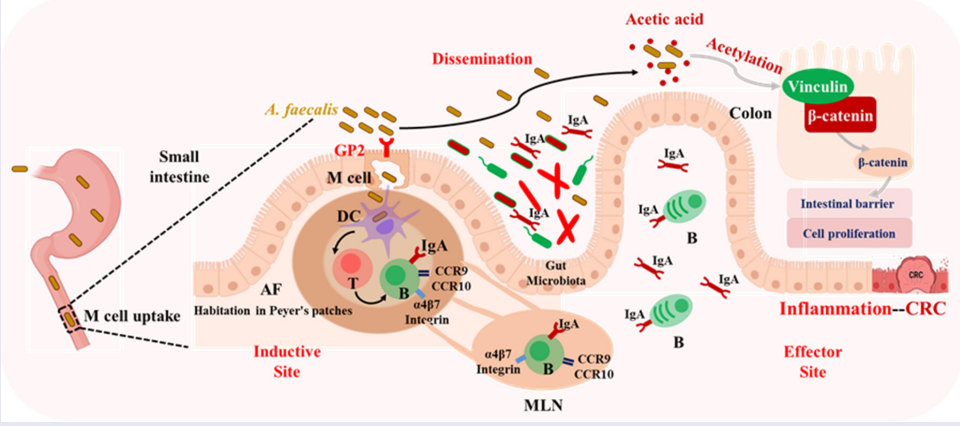

ARTICLE HISTORY
Received 16 September 2024
Revised 24 December 2024
Accepted 21 February 2025

KEYWORDS
Alcaligenes faecalis; peyer's patches; IgA; vinculin acetylation; inflammation-to-cancer transition

Introduction

Approximately 3.8×10^{13} gut microbiota[1] embedded in human gastrointestinal tract, played important roles in maintaining structural, immune, and metabolic homeostasis in gut.[2] Given the crucial role of gut microbiota on colon epithelial cells and innate immune system, overwhelming evidence demonstrated that the dysbiosis of gut microbiota formed a pro-carcinogenic microenvironment that is direct, central, and

CONTACT Linlin Lu lllu@gzucm.edu.cn State Key Laboratory of Traditional Chinese Medicine Syndrome, International Institute for Translational Chinese Medicine, Guangzhou, Guangdong 510006, China

*Present affiliation for Drs. Rong Zhang, Zhongqiu Liu and Linlin Lu is Chinese Medicine Guangdong Laboratory (Hengqin Laboratory), Guangdong Hengqin, 519000, China.

Supplemental data for this article can be accessed online at https://doi.org/10.1080/19490976.2025.2473511

essential for colorectal cancer(CRC).[3] Especially for patients bearing inflammatory bowel diseases (IBD), such as ulcerative colitis and crohn's disease, gut microbiota initially involved in the early stages of tumorigenesis triggered by long-lasting chronic inflammation.[4] Dysbiosis of gut microbiota significantly aggravated inflammation by promoting pro-inflammatory cytokines, altering immune cell functional response, and disrupting intestinal barrier integrity, which could ultimately facilitate CRC progression by causing DNA damage and genomic instability.[5] However, the precise mechanisms by which gut microbiota influences inflammation-to-cancer transition in CRC remain unclear.

Gut microbiota can be classified into four categories according to their locations: luminal commensal bacteria, mucosal-resident bacteria, epithelial-resident bacteria, and lymphatic-resident bacteria.[6] Numerous of evidence suggested that the first three categories of gut microbiota attributed to CRC progression by influencing both innate and adaptive immunity,[6] while innate immunity was considered as the key determinant in their impacts on CRC.[7] Meanwhile, unlike adaptive immunity, gut microbiota-triggered innate immunity occurred more rapidly and persisted consistently, from initiation of inflammation to malignant transformation.[8] Innate immune cells, such as dendritic cells (DCs), macrophages, and neutrophils, are predominantly located within four key gut-associated lymphoid tissues (GALTs): Peyer's patches, isolated lymphoid follicles (ILFs), mesenteric lymph nodes (MLNs), and intestinal lamina propria (ILP).[6] Peyer's patches are primary site for lymphatic-resident bacteria.[9] However, the molecular mechanisms by which lymphatic-resident bacteria in Peyer's patches influence the inflammation-to-cancer transition are not yet fully understood.

In Peyer's patches, *Alcaligenes spp*. constitute 72% of bacterial population, while in MLNs, *Alcaligenes spp*. represent only 4%.[10] *Alcaligenes faecalis* (*A. faecalis*), the main stain in *Alcaligenes spp*., might exert controversial effects on maintaining gut homeostasis. Previous results demonstrated that *A. faecalis* stimulated DCs to produce cytokines such as TGF-β, BAFF, and IL-6, which enhanced IgA generation and maintain mucosal immunity.[10] Meanwhile, *A. faecalis*-derived LPS, acted as TLR4 agonist, could promote IL-6 production without inducing excessive inflammation.[11] On the contrary, recent studies revealed that *A. faecalis* can translocate to blood and respiratory tract, disrupt immune homeostasis[12] and exacerbate inflammation progression.[13] In agreement, the ectopic localization of commensal bacteria played crucial role in CRC development. For instance, opportunistic pathobionts, such as *streptococcus bovis*, normally found in gastrointestinal tract, can invade and translocate into epithelial and endothelial cells, promoting CRC tumorigenesis.[14] However, the specific mechanisms by which *A. faecalis* influence inflammation-to-cancer transition remains unknown.

To explore the role of *A. faecalis* in inflammation-to-cancer transition, DSS-induced colitis model, $Apc^{Min/+}$ spontaneous adenoma model, and antibiotic clearance (ABX) model were utilized. We found that: i) *A. faecalis* could act as conditional pathogen to exacerbate colitis-associated carcinogenesis while exert no effect on normal intestinal homeostasis; ii) during colitis, the entry of *A. faecalis* into Peyer's patches was significantly reduced, leading to dramatic decrease in IgA^+ B cell and suppressed immune surveillance; iii) *A. faecalis* significantly increased acetylation of vinculin, which subsequently inhibited the binding ability of vinculin to β-catenin, ultimately impeded intestinal barrier integrity. In summary, our study revealed that during colitis, *A. faecalis* not only suppressed intestinal immune response by inhibiting IgA generation in Peyer's patches but also disrupted intestinal barrier via increasing vinculin acetylation, which simultaneously exacerbated inflammation-to-cancer transition. By revealing the first clue for understanding the critical role of *A. faecalis* in inflammation-to-cancer transition and dural role of *A. faecalis* in maintaining intestinal homeostasis, our study provided new insights into prevention of CRC in patients with IBDs.

Material and methods

Clinical samples

Colon cancer clinical tissue samples were provided by the Department of Anorectal Surgery, the First Affiliated Hospital of Guangzhou University of

Traditional Chinese Medicine. All patients had a histological diagnosis of colon cancer and had not received any previous treatment. Clinical and Pathologic Characteristics of Patients were shown Supplementary Table s1. Clinical trials were conducted after obtaining informed consent from the patients in accordance with the management regulations and requirements of Guangzhou University of Chinese Medicine (Ethics number: K-2023-010).

Animal experiments

To explore the effect of *A. faecalis* on colitis/carcinoma, we constructed a DSS-induced colitis model and an $Apc^{Min/+}$ mouse colon cancer model. 5–6 weeks old and male C57BL/6J mice ($n = 40$, 8/Group) were treated with a quadruple antibiotic (0.2 g/L ampicillin, neomycin and metronidazole and 0.1 g/L vancomycin) via drinking water for 3 days and then *A. faecalis* (1×10^9 CFU/mouse) was orally administered, and E.Coli was used as a negative control. Finally, the mouse colitis model was constructed by freely drinking 3% DSS for 8 days. 5–6 weeks old $Apc^{Min/+}$ mice ($n = 28$, 7/Group) and wild-type cagemates were obtained through self-propagation in the laboratory. Identification of mouse genotype was determined by agarose electrophoresis separation after specific PCR amplification and Genotype sequencing (Supplementary Figure S1I-J). 5–6 weeks old and male $Apc^{Min/+}$ mice were treated with a quadruple antibiotic (0.2 g/L ampicillin, neomycin, and metronidazole and 0.1 g/L vancomycin) via drinking water for 3 days, and then *A. faecalis* (1×10^9 CFU/mouse) was orally administered, and E. Coli was used as a negative control, and the bacteria were administered continuously for 10 weeks. Peyer's patches and colon tissue were harvested for subsequent experiments. All animal experiments were conducted in accordance with the Guangdong Provincial Laboratory Animal Management Guidelines and approved by the Animal Experiment Committee of the International Institute of Translational Medicine of Guangzhou University of Chinese Medicine (Permit number: SYXK(Guangdong)2019–0144).

RNA-seq

Different groups of Peyer's patches and colon tissues were collected. Total RNA was extracted for mRNA enrichment, then reverse transcribed into cDNA for library detection, and finally sequenced using Illumina PE150. Differential genes were screened out through gene expression levels, GO/KEGG enrichment, and transcription factor annotation. And immune cell typing was analyzed by Timer database.

Whole staining of Peyer's patches

FITC-D-Lys-labeled *A. faecalis* was injected into the ligated ileum containing single Peyer's patches, and after incubating for 1 h, the Peyer's patches tissue was removed and stained. FITC-D-Lys-labeled *A. faecalis* (Green), Gp2-labeled M cells (Red), DAPI-labeled Nuclei (Blue). Observed and photographed using FV1200MPE multicolor two-photon confocal microscope.

RNA FISH

Designed Cy3-labeled *A. faecalis*-specific probe (CTGCAGATACCGTCAGCAGT). First, paraffin sections with a thickness of 5 μL were prepared, followed by dewaxing, proteinase K digestion, and denaturation. Then placed them in a 37°C incubator to incubate the *A. faecalis*-specific probe for 12–16 h. Finally, incubated WGA (labeled Epithelial cells) and DAPI (labeled Nuclei) at room temperature in the dark. Observed and photographed using Leica TCS SP8 confocal microscope.

Statistical analysis

GraphPad Prism 8.0 software and SPSS 22 software were used, respectively, for graphing and statistical analysis. The normality of experimental data was tested using the Shapiro-Wilk method. One-way analysis of variance and Kruskal-Wallis H analysis were used for data that were normally distributed and those that were not normally distributed, respectively. Data in the legend represented mean±SEM.

The significance standards: $^{*}p < 0.05$, $^{**}p < 0.01$, $^{***}p < 0.001$.

Additional methods were provided in the Supplementary Materials.

Results

A. faecalis abundance and localization correlate with inflammation-to-cancer transition in colorectal cancer

The role of *A. faecalis* in intestine remains highly controversial due to the conflicting evidence on its dual effects, either inhibitory or promotive in inflammation. More importantly, few studies addressed the effects of *A. faecalis* on inflammation-cancer transition in colon carcinogenesis. Hence, we utilized DSS-induced mouse model to simulate colitis, AOM/DSS model, and $Apc^{Min/+}$ spontaneous intestinal adenoma model to mimic inflammation-mediated precancerous lesions. Additionally, 22 pairs of clinical samples were collected from CRC patients at stages I-IV (Supplementary Table S1). Using RNA FISH, the differences in abundance and localization of *A. faecalis* were determined in colon tissues during inflammation-to-cancer transition.

Compared to control, significant increase of *A. faecalis* abundance was observed in colon tissues of DSS-induced colitis, AOM/DSS, and more pronounced increase of *A. faecalis* were observed in $Apc^{Min/+}$ mice with intestinal adenomas. Unexpectedly, unlike in control where *A. faecalis* was sparsely attached to the apical side of intestinal villi, in DSS-induced colitis tissues, *A. faecalis* not only adhered to villi but also invaded into crypts. Moreover, as the pathological scenario progressed to pre-cancerous stage, *A. faecalis* was predominantly concentrated at the apical of villi (Figure 1(a)). These data suggested that the translocation and increased abundance of *A. faecalis* closely linked to inflammation-to-cancer transition in CRC.

To further verify whether *A. faecalis* can be enriched in tumor tissues and influence CRC progression, the abundance of *A. faecalis* was evaluated in CRC clinical tissues. *A. faecalis* could be detected either in tumor tissues or in the adjacent normal tissues, which included 5 cases with low *A. faecalis* expression and 17 cases with high *A. faecalis* expression (Figure 1(b)). And approximately 54.5% of tumor tissues harbored extremely higher levels of *A. faecalis* compared to the adjacent normal tissues ($p < 0.05$, Figure 1(b)). Furthermore, according RNA fluorescence shown in Figure 1(c), we found that abundance of *A. faecalis* gradiently increased with tumor stage progressed, which implied that *A. faecalis* may play a significant role in tumor progression, with its abundance positively correlating with tumor malignancy. Simultaneously, according RNA fluorescence shown in Figure 1(d), we found that abundance of *A. faecalis* gradiently increased during inflammation-to-cancer transition.

A. faecalis alone has no impact on physiological intestinal homeostasis, while during colitis, A. faecalis simultaneously suppressed intestinal immune response and disrupted intestinal barrier, which ultimately exacerbated colitis progression

To further confirm the impact of *A. faecalis* on colon tissues either in physiological or inflammatory circumstances, antibiotics clearance (ABX) animal model and DSS-induced colitis model were combined (Figure 2(a)). Compared to control, *A. faecalis* alone (C*A. faecalis*), without colitis, did not significantly affect the disease activity index (DAI, Figure 2(b)), colon length (Figure 2(c)), or colon appearance (Supplementary Figure S1F). When A. faecalis were given to mice bearing colitis simultaneously (M*A. faecalis*), *A. faecalis* could remarkably increase DAI by 1.5-fold ($p < 0.001$, Figure 2(b)), and dramatically shorten the colon length by 18.6% ($p < 0.001$, Figure 2(c,d)) compared to model. To further confirm how much does a single strain of *A. faecalis* contribute to inflammation, two models of DSS-induced colitis, with or without ABX, were constructed (Supplementary Figure S1A-1E). When most of gut microbiota was eliminated by antibiotics cocktail, *A. faecalis* could significantly enhance inflammation during colitis (Figure 2(b)). However, when other gut microbiota was present, the pro-inflammatory effect of *A. faecalis* was correspondingly reduced (Supplementary Figure S1C).

To further confirm the impact of *A. faecalis* on intestinal barrier function, the amount of high-molecular-weight FITC-dextran invade from

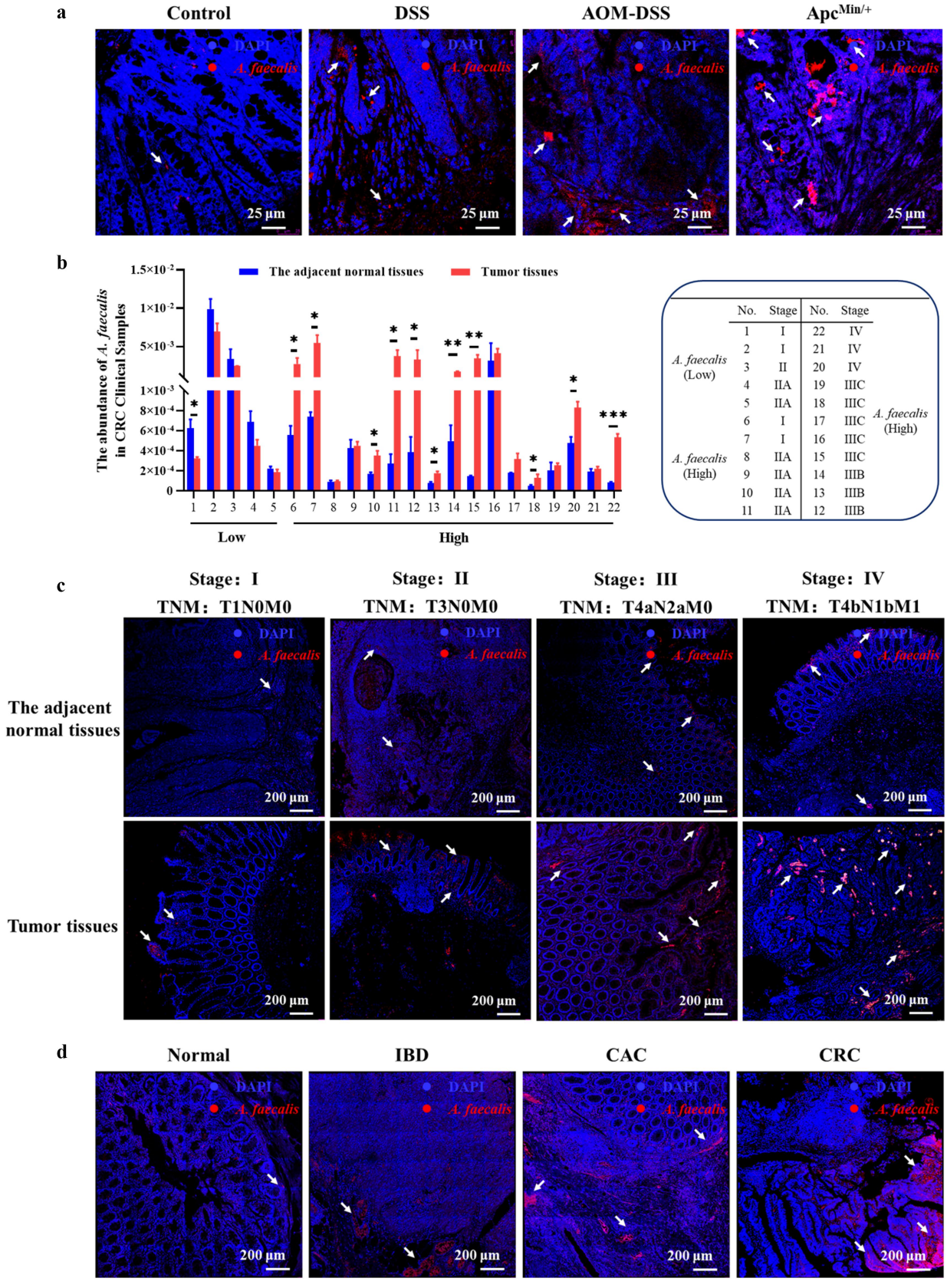

Figure 1. In inflammation, precancerous lesions, and CRC tumor tissues, the abundance of *A. faecalis* consistently increases, with a notable shift in their localization as well. (a) The abundance of *A. faecalis* in different stages during inflammation-to-cancer transition, ranging from physiological state (Control), inflammation (DSS-induced colitis), inflammation-to-cancer transition (AOM/DSS), and precancerous adenoma ($Apc^{Min/+}$) were detected by RNA FISH. *A. faecalis* was labeled in red, dapi-labeled nuclei in blue. Scale bar:

intestine into blood was measured. As shown in Figure 2(e,f), C*A. faecalis* did not significantly affect intestinal barrier, whereas M*A. faecalis* further aggravated barrier dysfunction induced by colitis. AB-PAS staining revealed that in M*A. faecalis*, the structure of colon epithelial cells was extensively disrupted, and mucus content in glandular lumen was significantly decreased (Figure 2(g)). Compared to model, the number of Peyer's patches was significantly reduced in M*A. faecalis* (Figure 2(h)). Furthermore, during colitis, a near-complete loss of GC area in Peyer's patches was found in M*A. faecalis* (Figure 2(i), supplementary figure S1G-H and Figure 2(i) Control as an example to show the structure of mouse Peyer's patches).

To examine the effect of *A. faecalis* on inflammation-to-cancer transition, inflammation-involved $Apc^{Min/+}$ mice model was applied (Figure 2(j) and supplementary figure S1I-1J). Compared to model, *A. faecalis* significantly increased tumor size ($p < 0.05$, Figure 2(k–l)). Additionally, the structural integrity of Peyer's patches, especially for SED and GC area, was almost destroyed after exposed to *A. faecalis* (Figure 2(m) and supplementary figure S1K), and AB-PAS staining also showed that mucous layer was markedly disrupted in M*A. faecalis* (Figure 2 (n)). Furthermore, to further determine the effect of *A. faecalis* on cancer progression, HCT116 xenograft model and orthotopic colon cancer model were also utilized. As shown in supplementary figure S2, *A. faecalis* also remarkably promoted tumor growth ($p < 0.05$).

A. Faecalis exacerbated the progression of colitis to carcinoma by translocating from Peyer's patches in intestine to colon epithelium

By labeling *A. faecalis* with fluorescent dye FITC-D-Lys and tracked its real-time fluorescence, the differences of *A. faecalis* entry into Peyer's patches via M cells, either in the presence or absence of colitis, were determined (Figures 3(a,b)). We found that the green fluorescent *A. faecalis* co-localized with the red-labeled M cells (Figures 3(c,d)), indicating that *A. faecalis* indeed entered Peyer's patches via M cells. Compared to control, *A. faecalis* alone (C*A. faecalis*) did not significantly affect the distributed abundance of M cells in Peyer's patches. In contrast, during colitis, *A. faecalis* remarkably reduced the green fluorescence of M cells in M*A. faecalis* compared to that in model (Figure 3(e)). Additionally, in situ hybridization for *A. faecalis* revealed that most of *A. faecalis*, upon entering Peyer's patches, abundantly accumulated in secondary lymphoid follicle, which are main areas for dendritic cells (DCs). These results suggested that under physiological conditions, *A. faecalis* might enter Peyer's patches via M cells and reside within DCs to maintain intestinal immune homeostasis. However, during colitis, the entry ability and resident abundance of *A. faecalis* in Peyer's patches were decreased, leading to dysfunctional immune response (Figure 3(e)).

As showed previously, the entry of *A. faecalis* into Peyer's patches was reduced significantly, where did the translocated *A. faecalis* colonize in intestinal lumen? To determine the destination of *A. faecalis*, colon tissues, located at bottom of small intestine, were collected and co-localized of *A. faecalis* and epithelial cells labeled by WGA. As showed in Figure 3(f), *A. faecalis* significantly implanted and accumulated in colon epithelium. In model with colitis, the disrupted intestinal barrier allowed more *A. faecalis* to infiltrate colon epithelium, particularly colonized in crypts (Figure 3(f)). Furthermore, in $Apc^{Min/+}$ adenoma mice model, we also found notable reduction of

25 μm. (b) The abundance of *A. faecalis* in 22 pairs of clinical CRC tissues were measured by qPCR, and clinical samples are sorted by tumor stage. (c) The abundance of *A. faecalis* in different stages of CRC (stage I, T1N0M0; stage II, T3N0M0; stage III, T4aN2aM0; stage IV: T4bN1bM1) was analyzed by RNA FISH. *A. faecalis* was labeled showed in red, dapi-labeled nuclei in blue. Scale bar: 200 μm. *$p <$ 0.05, **$p < 0.01$, ***$p < 0.001$: the significance of CRC tumor tissues vs the adjacent normal tissues. (d) The abundance of *A. faecalis* in different stages during inflammation-to-cancer transition, ranging from clinicopathological (Normal), inflammation (IBD), inflammation-to-cancer transition (CAC), and adenoma (CRC) were detected by RNA FISH. *A. faecalis* was labeled in red, dapi-labeled nuclei in blue. Scale bar: 200 μm.

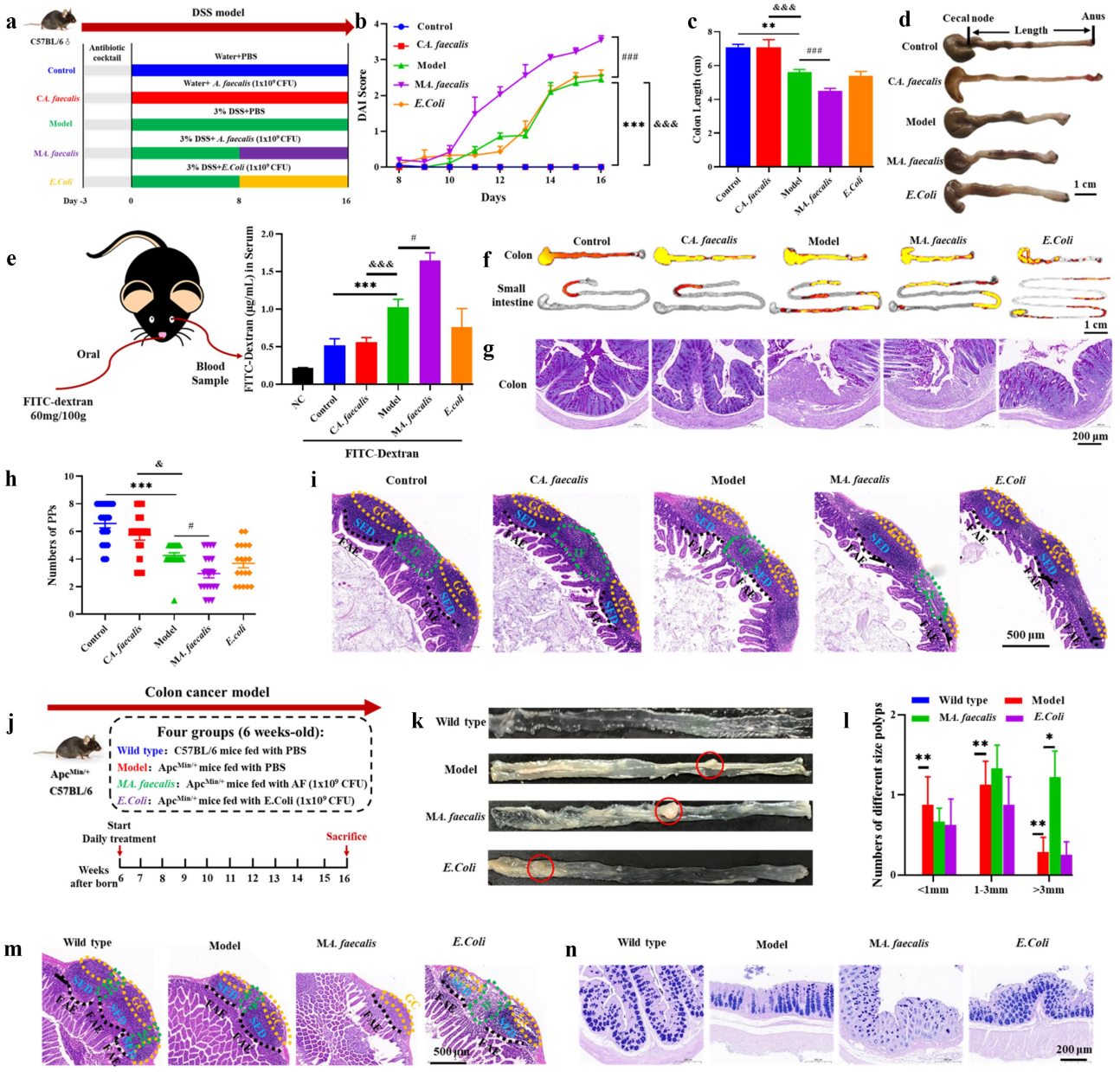

Figure 2. *A. faecalis* alone exerted no effects on intestinal homeostasis under physiological conditions while aggravated DSS-induced colitis and inflammation-to-cancer transition via disrupting intestinal barrier and suppressing immune response in Peyer's patches. (a) Schematic diagram of DSS-induced colitis mice model. *A. faecalis* was administrated without or with colitis, which refers to control combined with *A. faecalis* (C*A. faecalis*) and model combined with *A. faecalis* (M*A. faecalis*), respectively. (b) Disease activity index during DSS-induced colitis. (c) Statistical analysis of colon length. (d) Representative images for colon appearance. (e) FITC-D levels in serum. (f) Representative images of small intestine and colon by fluorescence imaging. (g) Representative images of colon AB-PAS staining, scale bar: 200 μm. (h) The numbers of Peyer's patches (Peyer's patches) in mice intestine. (i) Representative HE staining images of Peyer's patches, follicle associated epithelium (FAE), sub-epithelial dome (SED), interfollicular region (IF), and germinal center (GC). Scale bar: 500 μm. (j) Schematic diagram of $Apc^{Min/+}$ colon adenoma model. (k) Representative images of colon tumors in $Apc^{Min/+}$ mice. (l) The numbers and sizes of colon tumors in $Apc^{Min/+}$ mice, compared to model, $^{*}p < 0.05$, $^{**}p < 0.01$. (m) Representative HE staining images of Peyer's patches. Scale bar: 500 μm. (n) Representative images of colon AB-PAS staining, scale bar: 200 μm. Statistical significance: control vs model: $^{**}p < 0.01$, $^{***}p < 0.001$. C*A. faecalis* vs model: $^{\&}p < 0.05$, $^{\&\&\&}p < 0.001$. M*A. faecalis* vs model: $^{\#}p < 0.05$, $^{\#\#\#}p < 0.001$.

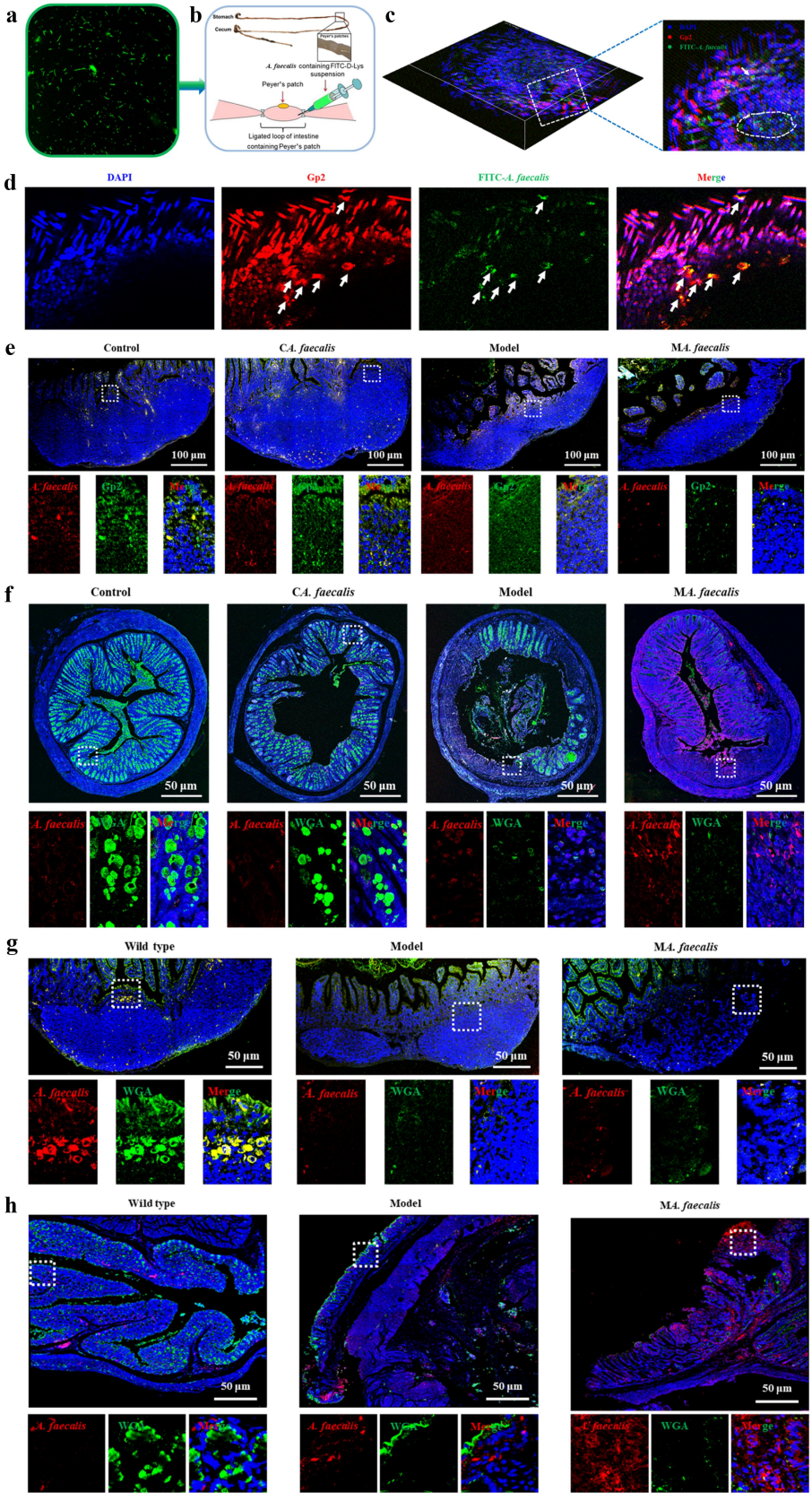

Figure 3. The amount of *A. faecalis* was decreased in Peyer's patches of intestine while increased in colon both in DSS-induced colitis and $Apc^{Min/+}$ adenoma mice model. (a) FITC-D-Lys-labeled *A. faecalis* in vitro. (b) Ligated loop of intestine containing Peyer's patches model. (c-d) three-dimensional images of multicolor two-photon confocal microscopy showing FITC-D-Lys-labeled *A. faecalis* (green), Gp2-labeled M cells (red), and dapi-labeled nuclei (blue). Scale bar: 50 μm. (e) Representative images of *A. faecalis* RNA FISH in Peyer's

A. faecalis in Peyer's patches, and significant increase of *A. faecalis* at colon segment in M*A. faecalis* (Figure 3(g,h)).

A. faecalis reduced B cells function in Peyer's patches and inhibited IgA+ B cells homing to the intestine

Peyer's patches are essential follicular structures that mediate intestinal mucosal immunity. Our previous data demonstrated a significant reduction in the entry of *A. faecalis* into Peyer's patches during colitis; therefore, RNA sequencing (RNA-seq) and immunofluorescence co-localization were utilized to elucidate the correlation between *A. faecalis* presence in Peyer's patches and the immune response. In the DSS-induced colitis, dramatic reduction in B cells and significant increase in other immune cells were observed, indicating that colitis progression might be closely associated with B cell depletion in Peyer's patches. During colitis, the diminished entry of *A. faecalis* into Peyer's patches further decreased B cells, downregulated DCs, and inversely increased macrophages. Additionally, *A. faecalis*-associated colitis promoted the migration of neutrophils to Peyer's patches from intestinal lumen, further contributing to the inflammatory response (Figure 4(b)). Compared to DSS-induced colitis model, *A. faecalis*-mediated colitis (M*A. faecalis*) significantly impaired the function of most immune cells. This impairment was most pronounced in DCs, B cells, and T cells, with an average reduction in functional markers exceeding 80% in the context of *A. faecalis*-mediated colitis (Figures 4(a)).

The co-localization of *A. faecalis* and $CD11c^+$ DCs suggested that *A. faecalis* could reside within DCs after entering Peyer's patches (Figure 4(d) and Figure 3(g) Wild type as an example to show that A. faecalis was taken up by DCs). Compared to model, significant reduction in DCs was observed in *A. faecalis*-mediated colitis (M*A. faecalis*) (Figure 4(e)). *A. faecalis* alone (C*A. faecalis*) significantly triggered the proliferation of IgA+ B cells, while in the context of colitis, IgA+ B cells were markedly diminished in M*A. faecalis* (Figure 4(f)). Immunofluorescence results also revealed that during colitis, *A. faecalis* decreased the intensity of $B220^+$ memory B lymphocytes and increased that of $CD138^+$ plasma cells (Supplementary figure S3A). Moreover, the expressions of gut-homing receptors, such as integrin α4β7, CCR9, and CCR10, were determined in Peyer's patches and mesenteric lymph nodes (MLNs), two critical sites in gut-associated lymphoid tissue, respectively. Compared to model, M*A. faecalis* exhibited reduced intensity of integrin α4β7, CCR9, and CCR10 (Figure 4(g)). Consistently, the number of IgA+ B cells migrating to colon tissues was significantly reduced in M*A. faecalis* compared to model (Figure 4(h)). Meanwhile, *A. faecalis* markedly reduced intensity of $CD4^+$ T cells and enhanced that of $CD8^+$ T cells compared to model (Supplementary figure S3B).

A. Faecalis obstruction in Peyer's patches led to IgA reduction in colon and microbial dysbiosis, promoting intestinal inflammation

Secretory IgA could adhere to intestinal pathogens and maintain intestinal homeostasis, and our previous findings revealed *A. faecalis* significantly suppressed IgA+ B cells in Peyer's patches, the proportion of IgA in colon segment was also decreased in M*A. faecalis* (Figure 5(a,b)). Since *A. faecalis* could translocated from Peyer's patches to colon, how did *A. faecalis* impact gut microbiota in colon? Using 16S rDNA sequencing, we examined the changes in microbial diversity within colon during colitis. As showed in Figure 5(c), the profile of gut microbiota was diverse between model and M*A. faecalis*, especially in reduced Chao1

patches of DSS model showing *A. faecalis* (red), Gp2-labeled M cells (green), and dapi-labeled nuclei (blue). Scale bar: 100 μm. (f) Representative images of *A. faecalis* RNA FISH in the colon of DSS model showing *A. faecalis* (red), wga-labeled epithelial cells (green), and dapi-labeled nuclei (blue). Scale bar: 50 μm. (g) Representative images of *A. faecalis* RNA FISH in Peyer's patches of $Apc^{Min/+}$ model showing *A. faecalis* (red), Gp2-labeled M cells (green), and dapi-labeled nuclei (blue). Scale bar: 50 μm. (h) Representative images of *A. faecalis* RNA FISH in the colon of $Apc^{Min/+}$ model showing *A. faecalis* (red), wga-labeled epithelial cells (green), and dapi-labeled nuclei (blue). Scale bar: 50 μm.

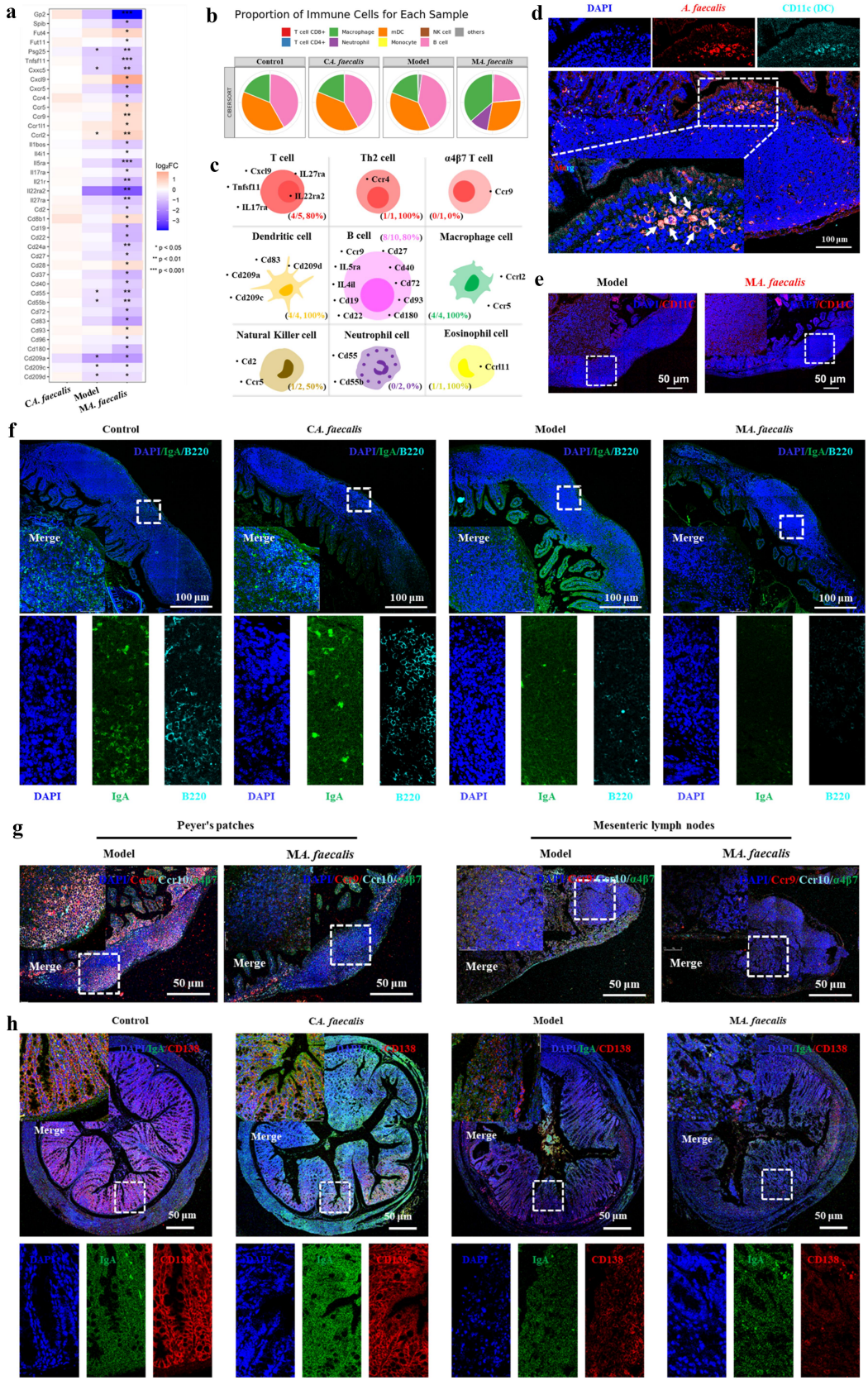

Figure 4. *A. faecalis* altered immune cell dynamics in Peyer's patches and exacerbated colitis. (a) Differentially expressed immune cytokines and chemokines in Peyer's patches. (b) Analysis of the proportion of immune cells in Peyer's patches using the timer database. (c) Annotation of major immune cells in Peyer's patches. (d) *A. faecalis* captured by DCs. *A. faecalis* (red), CD11c-labeled DCs (cyan), dapi-labeled nuclei (blue), scale bar, 100 μm. (e) Representative images of DC immunofluorescence in Peyer's patches. CD11c-

(Figures 5d) and Shannon index (Figures 5e). Consequently, *A. faecalis* translocation significantly decreased the abundance of *Bacteroidetes* and increased that of *Proteobacteria*. Notably, compared to model, M*A. faecalis* showed a reduced abundance of probiotic *Muribaculaceae* and an increased abundance of pathogens such as *Staphylococcus*, *Escherichia-Shigella*, and *Corynebacterium* (Figures 5(f–g)). *A. faecalis* translocation led to substantial shifts in the bacterial community composition, resulting in dysbiosis. KEGG pathway enrichment analysis revealed that *A. faecalis* translocation primarily invades intestinal epithelial cells and was associated with immune system-related diseases (Figures 5(h,i)).

A. faecalis enriched in colon increased vinculin acetylation and promoted inflammation-to-carcinoma transition

By using UPLC-TQMS, *A. faecalis*-associated metabolites enriched in colon tissues were examined. As showed in Figure 6(a), the specific differential metabolites in M*A. faecalis* were primarily enriched in SCFAs (66.67%), followed by organic acids (26.67%) and fatty acids (6.67%). Acetic acid level in C*A. faecalis* was comparable to control, while when subjected to *A. faecalis*-associated colitis, acetic acid level in M*A. faecalis* was significantly higher compared to model (Figure 6(b)).

Previous study indicated that gut microbiota generated SCFAs, which extensively participated in post-translational modifications (PTMs) of intestinal epithelial cells, directly influencing cancer process.[15] Compared to model, significant increase in acetylation (Kac) level was observed in M*A. faecalis* (Figure 6(c) and supplementary Figure S4A-4B). Furthermore, Kac levels were found extremely high either in DSS-induced colitis mice, $Apc^{Min/+}$ mice model or in six pairs of CRC clinical tissues (Figure 6(c)). Subsequently, differentially modified protein peptides were identified using 4D-label free quantitative acetylproteomics. Among 65 significantly downregulated peptides (FC < 0.5, $p < 0.05$) and 27 upregulated peptides (FC > 2.0, $p < 0.05$), the most significantly upregulated peptide belong to vinculin (Figure 6(d)). In pan-cancer tissues, the expression of vinculin remarkably decreased in tumors compared to normal tissues (Figures 6(e)). In CRC tissues, vinculin was significantly downregulated at both gene and protein levels (Figure 6(f,g)). In *A. faecalis*-associated colitis and adenoma tissues, the expression of vinculin was decreased while Kac level was increased in M*A. faecalis* compared to model (Figure 6(h–j) and supplementary figure S4D-4E). Whereas, under physical conditions, vinculin protein and Kac levels were unaffected in C*A. faecalis* compared to control (Figure 6(h)).

Additionally, the protein expression of tight junction proteins ZO1 and Claudin1, as well as adhesion proteins E-cadherin were significantly reduced in *A. faecalis*-associated DSS-induced colitis model and $Apc^{Min/+}$ spontaneous adenoma model, suggesting *A. faecalis* could disrupt tight junctions, exacerbate intestinal barrier damage to participate in inflammation-to-cancer transition (Figure 6(I–k)). Immunofluorescence revealed an inverse relationship between vinculin and β-catenin in M*A. faecalis*, as well as decreased cytoplasmic β-catenin and increased nuclear β-catenin in M*A. faecalis* (Figure 6(l–n)). Ki67 staining indicated increased cell proliferation in M*A. faecalis* compared to model (Figure 6(m–o)), suggesting that nuclear translocation of β-catenin promoted tumor development. In conclusion, our findings suggested that when *A. faecalis* translocated from Peyer's patches to colon tissues, the vinculin acetylation in colon epithelial cells were increased, which may disrupt tight and adhesion junctions embedded in intestinal barriers, ultimately promote inflammation-to-cancer transition.

labeled DCs (red), dapi-labeled nuclei (blue), scale bar, 50 μm. (f) Representative images of IgA and B220 immunofluorescence in Peyer's patches. IgA (green), B220-labeled B cells (cyan), dapi-labeled nuclei (blue), scale bar, 100 μm. (g) Representative images of intestinal homing receptors α4β7, CCR9, and CCR10 immunofluorescence in Peyer's patches and MLNs. α4β7 (green), CCR9 (red), CCR10 (cyan), dapi-labeled nuclei (blue), scale bar, 50 μm. (h) Representative images of IgA and CD138 immunofluorescence in Peyer's patches. IgA (green), CD138-labeled effector B cells (red), dapi-labeled nuclei (blue), scale bar, 50 μm.

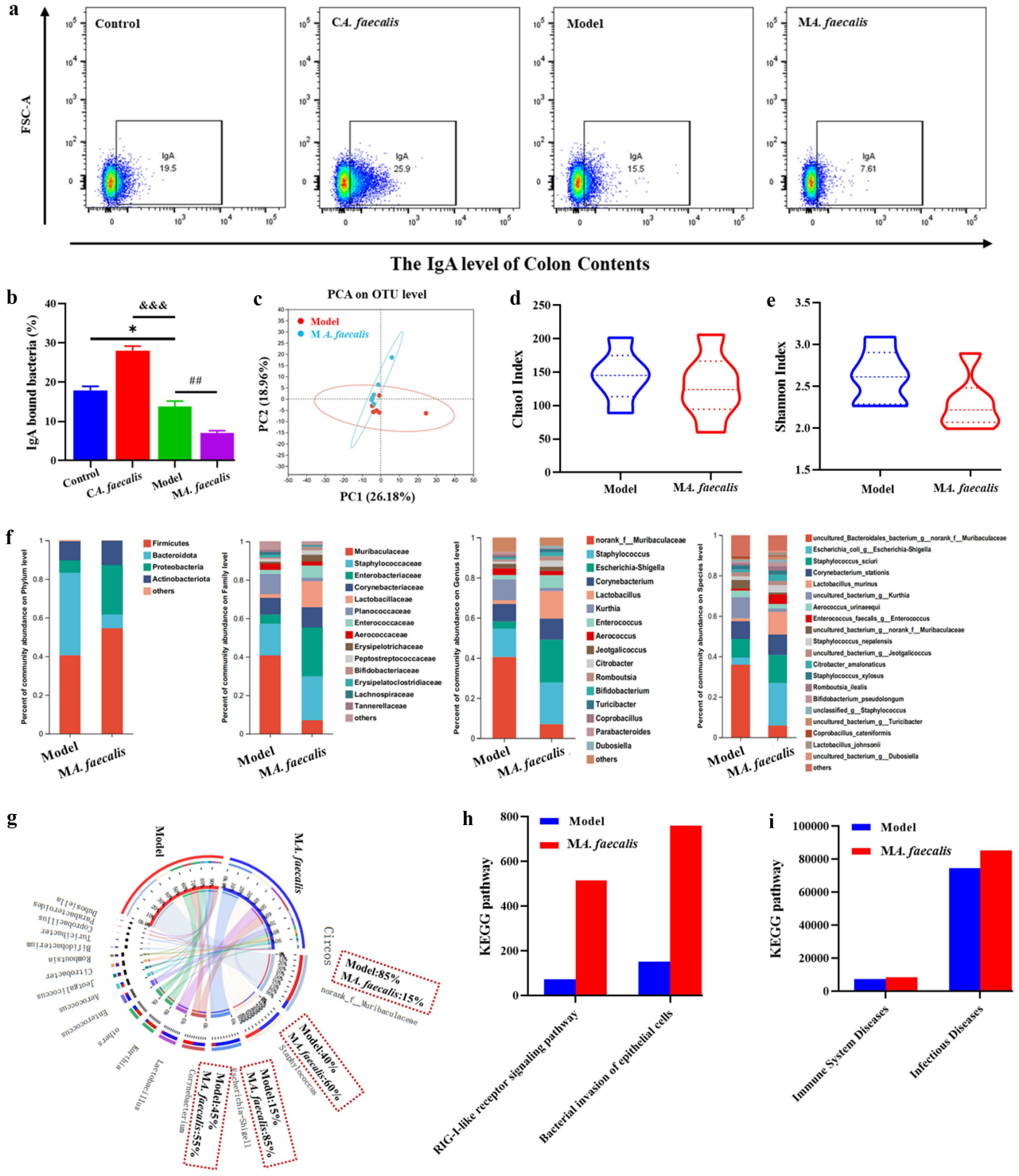

Figure 5. *A. faecalis* induced gut microbiota disorder, decreasing beneficial bacteria and increasing harmful bacteria. (a-b) IgA levels in colon contents measured by flow cytometry, with CD138-labeled plasma cells. (c) PCA analysis of gut microbiota. (d) Chao1 diversity index. (e) Shannon diversity index. (f) Taxonomic analysis of microbiota at the phylum, family, genus, and species levels. (g) Circos visualization diagram of microbiota at the genus level. (h-i) KEGG pathway analysis.

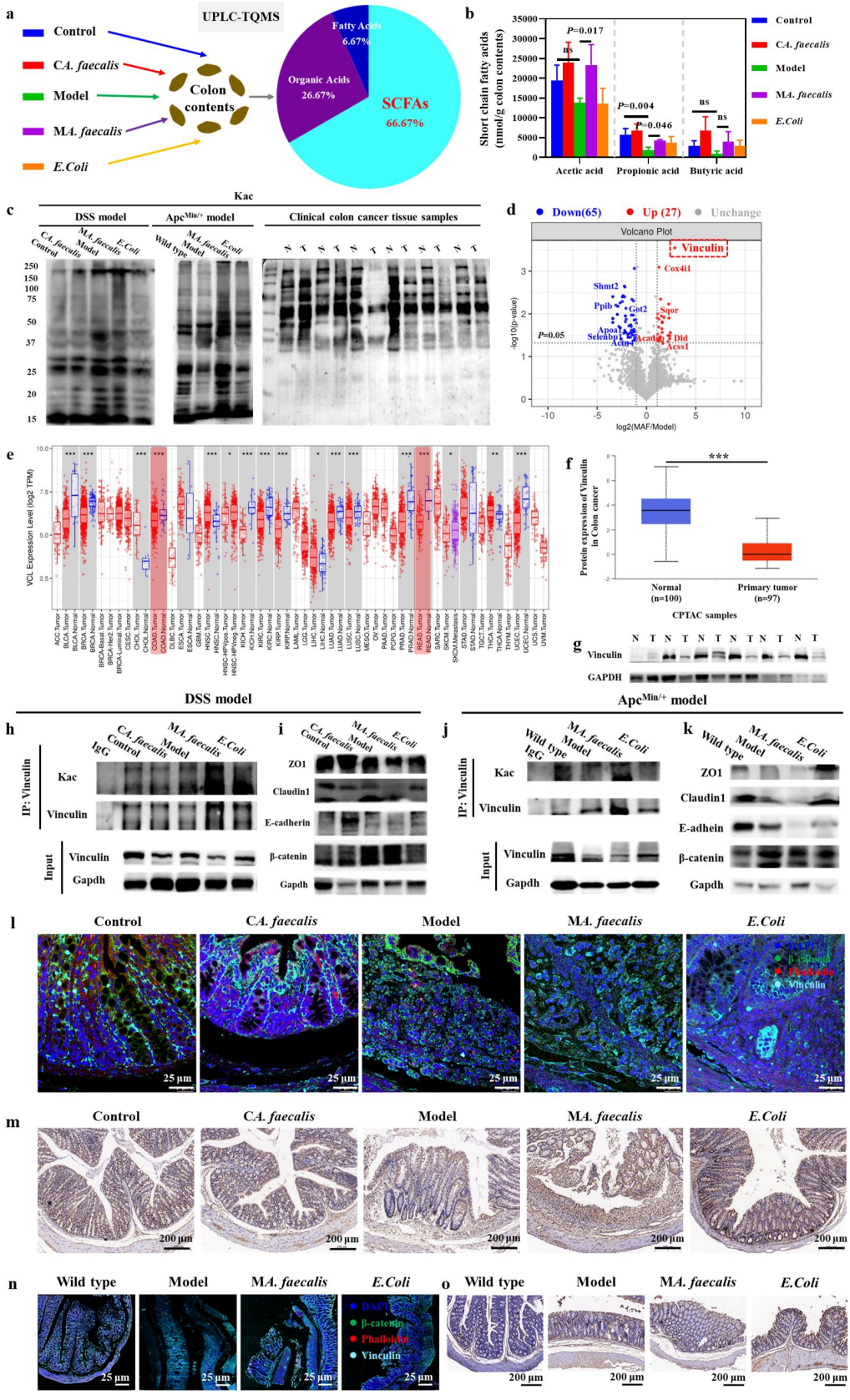

Figure 6. *A. faecalis* increased vinculin acetylation and promoted colitis-to-carcinoma transition. (a) Metabolites in the intestinal contents detected by UPLC-TQMS technology. (b) Main metabolites of SCFAs in intestinal contents. (c) PTMs (kac) in the DSS model, $Apc^{Min/+}$ model, and clinical colon cancer tissue samples. (d) Volcano plot of modified protein peptides. (e) Differential expression of vinculin between tumor and adjacent normal tissue in COAD and READ analyzed by the DiffExp module of the timer database. (f)

A. faecalis-derived acetate increased vinculin acetylation to promote colorectal carcinogenesis

To investigate the mechanism of action of *A. faecalis*-derived acetate to promote colorectal carcinogenesis, we first used LC-MS to detect the acetic acid level in the TSB, *A. faecalis*, inactivated *A. faecalis*, *A. faecalis* supernatant, and inactivated *A. faecalis* supernatant. We found that acetic acid level in inactivated *A. faecalis* was significantly higher compared to TSB (Figure 7(a)). Then, we used CCK8 to examine the cell viability of acetate on the colon cancer cell line HCT-116, as showed in Figure 7(b), the IC50 values were 96.83 mm at 24 h and 33.42 mm at 48 h. Next, We used IP and WB to examine the effect of acetate on Vinculin acetylation, and the results showed that Vinculin Kac level was increased at 33.42 mm of acetate compared to Control (Figure 7(c)). Acetylation is produced by KATs (including P300, GCN5, PCAF, SCR3, et al.) transferring an acetyl group from acetyl-CoA to the ε-amino side chain of lysine, and participates in the regulation of important molecules, thereby regulating the disease process (Figure 7(d)). Through protein-protein docking, we found that Vinculin protein and P300 protein could be very likely to bind (Figure 7(e)). At the same time, P300 expression level increased and intracellular acetyl-CoA level increased after acetate treatment (Figure 7(f–g)).

Furthermore, by analyzing the COAD data, it was found that the correlation coefficient r between Vinculin (VCL) and β-catenin (CTNNB1) was 0.28 ($p < 0.001$), indicating that VCL was significantly related to WNT (Figure 7(h)). In addition, GSEA enrichment analysis that the transcriptome of VCL high-expression samples was enriched in intestinal diseases (Figure 7(i)), and was significantly positively correlated with the WNT signaling pathway. (Figure 7(j), NES = 1.24, padj < 0.05). To examine the relationship between Vinculin acetylation and β-catenin, we used acetate and IWR-1-endo (β-catenin inhibitor) to treat the colon cancer cell line HCT-116. Immunofluorescence results were shown in Figure 7 (k–l), compared with Control, after treatment with acetate alone, the acetylation level increased significantly, and the ratio of nuclear translocation of β-catenin significantly increased by approximately 40% (***$p < 0.001$). Compared with IWR-1-endo, after treatment with acetate and IWR-1-endo together, the acetylation level was significantly increased, and the ratio of nuclear translocation of β-catenin slightly increased by approximately 7% ($p > 0.05$, ns). Similarly, we also found that, compared with Control, after treatment with acetate alone, the ratio of HCT-116 cells migration ability significantly increased by approximately 50%. Compared with IWR-1-endo, after treatment with acetate and IWR-1-endo together, the ratio of HCT-116 cells migration ability increased by approximately 10% (Figure 7(m, n)). In general, as acetylation increased, nuclear translocation of β-catenin increased, resulting in more cell migration.However, when β-catenin was inhibited, although increased acetylation resulted in increased n nuclear translocation of β-catenin, cells migrated no more than in the presence of β-catenin. This indicated that cell migration relied on increased acetylation to promote nuclear translocation of β-catenin to promote tumor progression.

Discussion

The phenotypic differences and molecular mechanisms by which intestinal lymphoid tissue-resident commensal bacteria impact disease progression remain unclear. Our study identified *A. faecalis*, a conditional pathogen residing in Peyer's patches, could suppress mucosal immune responses via reducing IgA^+ B cells in Peyer's patches and disrupt intestinal barrier via increasing vinculin acetylation in colon epithelial cells, ultimately promoting inflammation-to-cancer transition.

Expression level of vinculin protein in TCGA colon cancer. Normal vs primary tumor, ***$p < 0.001$. (g) Detection of vinculin protein expression level in colon cancer clinical samples by Western blotting. (h, j) vinculin protein and kac level by Western blotting in DSS model and $Apc^{Min/+}$ model. (i, k) protein levels of ZO1, Claudin1, E-cadherin, and β-catenin in the colon by Western blotting in DSS model and $Apc^{Min/+}$ model. (l, n) immunofluorescence of vinculin protein and β-catenin protein in DSS model and $Apc^{Min/+}$ model. β-catenin (green), phalloidin-labeled cytoskeleton (red), vinculin (cyan), dapi-labeled nuclei (blue), scale bar, 25 μm. (m, o) Representative images of colon Ki67 immunohistochemistry in DSS model and $Apc^{Min/+}$ model, scale bar, 25 μm.

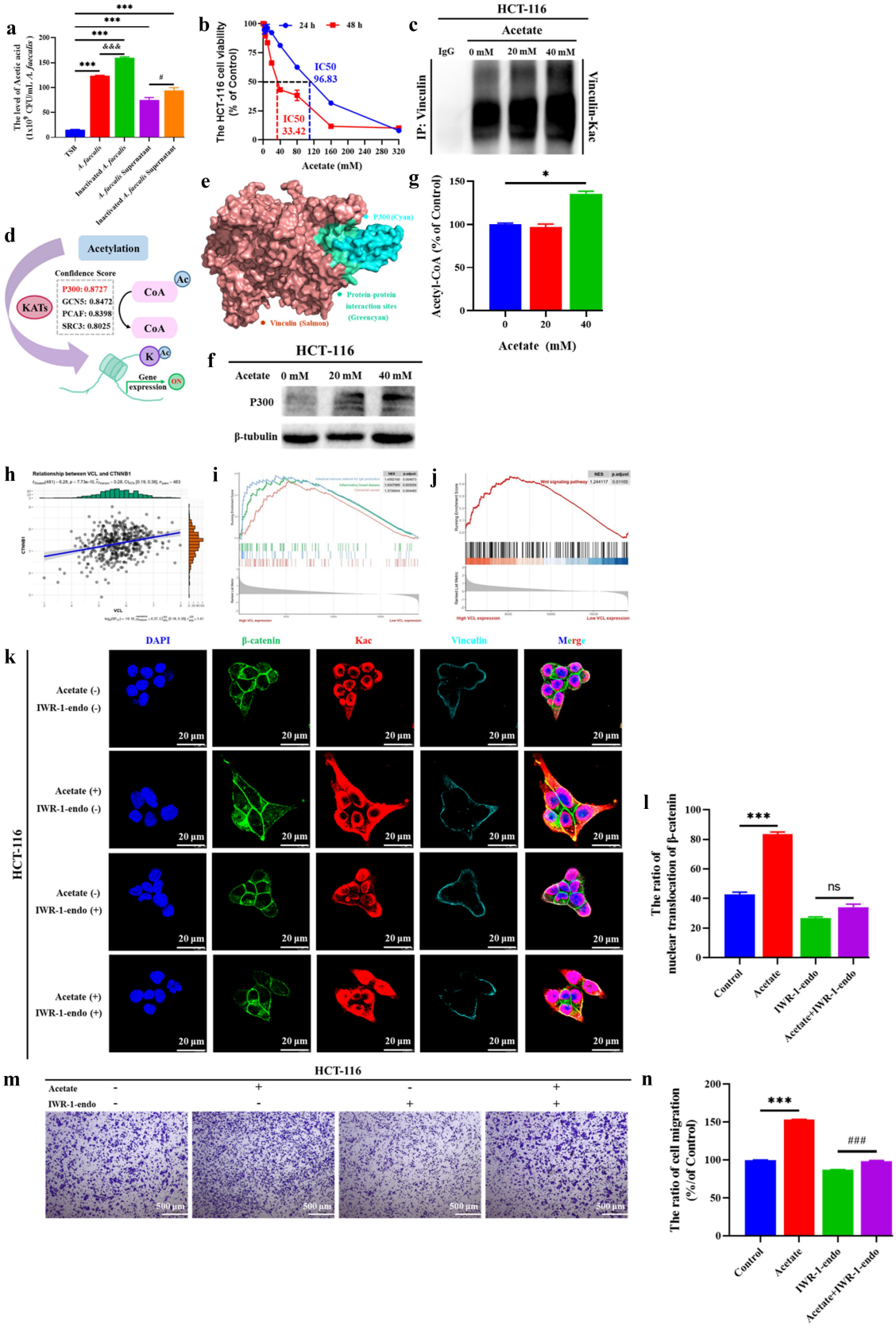

Figure 7. *A. faecalis*-derived acetate increased vinculin acetylation to promote colorectal carcinogenesis. (a) The acetic acid level in the TSB, *A. faecalis*, inactivated *A. faecalis*, *A. faecalis* supernatant, and inactivated *A. faecalis* supernatant detected by LC-MS technology. Compared to TSB, $^{***}p < 0.001$. *A. faecalis* vs inactivated *A. faecalis*: $^{\&\&\&}p < 0.001$. *A. faecalis* supernatant vs inactivated *A. faecalis* supernatant: $^{\#}p < 0.05$. (b) HCT-116 cells were treated with acetate (0, 2.5, 5, 10, 20, 40, 80, and 320 mm) for 24 and 48 h, and the

Our study demonstrated A. faecalis, acted as a conditional pathogen, exacerbated colitis and promoted carcinogenesis under inflammatory conditions while exert no effects under normal conditions

Previous study revealed *A. faecalis*-derived LPS could serve as a nasal vaccine adjuvant to active immune response without aggravate inflammation,[11,16] while other studies suggested *A. faecalis* could trigger inflammation. Combining DSS model with $Apc^{Min/+}$ spontaneous adenoma model, we initially explored the impact of *A. faecalis* on inflammation-to-cancer transition. Interestingly, our findings demonstrated that *A. faecalis* alone could effectively maintain physiological intestinal homeostasis via embedding in Peyer's patches and activating mucosal immune surveillance (Figure 2). However, during DSS-induced colitis, *A. faecalis* dramatically exacerbated colitis and promoted adenoma formation in $Apc^{Min/+}$ mice (Figure 2 and supplementary figure S1). Our findings highlighted the context-dependent effects of gut microbiota, where the same bacterial specie could have protective role under homeostatic condition but become pathogenic in the context of inflammation.

Our study revealed that the translocation of A. faecalis from Peyer's patches to colon, significantly reduced IgA+ B cells in Peyer's patches, leading to a decrease of IgA in colon tissues, which ultimately suppressed intestinal mucosal immune responses

Consistent with previous findings by Obata et al ,[10,17] we also found *A. faecalis* could be taken up by M cells to enter Peyer's patches (Figure 3). The absence of mature $Gp2^+$ M cells impeded trafficking of antigens, which hindering the initiation of mucosal immune response.[18] We found that during colitis, *A. faecalis* significantly reduced mature $Gp2^+$ M cells, thereby impairing the ability of M cells to take up antigens, resulting in the immune cells embedded in Peyer's patches were unable to trigger immune response (Figure 3). Most importantly, since *A. faecalis* could not invade into Peyer's patches, more *A. faecalis* can colonize in colon tissues with intestinal movement (Figure 4). Meanwhile, during colitis, *A. faecalis* altered the profile of immune cells in Peyer's patches, especially for IgA+ B cells (Figure 4). Previous studies demonstrated M cells depletion might significantly attribute to GC diminish and low level of IgA.[19] Consistently, IgA+ B cells both in intestine and colon was reduced after *A. faecalis* treatment (Figure 4). Secreted IgA (SIgA) could bind to commensal microbiota as part of innate immune surveillance[20], our findings also showed that reduced IgA levels correlate with increased microbial dysbiosis (Figure 4). *A. faecalis*'s presence under inflammatory conditions not only exacerbated colitis but also facilitated the migration of *A. faecalis* to the colon, where it disrupted the microbial community.

Our study concluded that A. faecalis significantly increased vinculin acetylation, which disrupted intestinal barrier integrity, promoting inflammation-to-cancer transition

Gut is a unique site of host-microbe interactions, where microbially-derived small molecules such as SCFAs are key modulators for maintaining intestinal homeostasis. Our data revealed that during colitis, *A. faecalis* could translocate from the small intestine to colon, and disrupt microbial homeostasis in colon as well. Does *A. faecalis* translocation influence SCFA production and

percentages of viable cells were measured by CCK8 assays. (c) The expression of vinculin-Kac in the HCT-116 with acetate (0, 20, 40 mm) treatment for 48 h. (d) Schematic diagram of the acetylation process. (e) Vinculin protein and P300 protein docking, vinculin (salmon), P300 (cyan), Protein-Protein interaction sites (greencyan). (f) The expression of P300 protein in the HCT-116 with acetate (0, 20, 40 mm) treatment for 48 h. (g) The intracellular acetyl-CoA level in the HCT-116 with acetate (0, 20, 40 mm) treatment for 48 h. acetate (0 mm) vs acetate (40 mm): $^{\#}p < 0.05$. (H) The relationship between vinculin (VCL) and β-catenin (CTNNB1) was analyzed by the COAD data. (i-j) the relationship between vinculin (VCL) and intestinal diseases was analyzed by the GSEA. (k) Immunofluorescence of Kac, vinculin protein, and β-catenin protein in the HCT-116 with acetate (0, 20, 40 mm) treatment for 48 h. β-catenin (green), Kac (red), vinculin (cyan), dapi-labeled nuclei (blue), scale bar, 20 μm. (l) The ratio of nuclear translocation of β-catenin. (m) Cell migration ability was measured by transwell assays, scale bar, 500 μm. (N) The ratio of cell migration (%/of control).

contribute to colitis-associated cancer progression? We found among other differentially enriched SCFAs, acetic acid was the most significantly increased metabolites in *A. faecalis*-associated colitis. Recent study demonstrated that SCFAs could influence various PTMs to participate in cancer progression.[21] Our further study revealed that *A. faecalis* significantly altered the PTMs landscape in intestinal epithelial cells. Most importantly, we found that vinculin acetylation was extremely higher. Previous study revealed that vinculin acetylation could disrupt the E-cadherin/β-catenin complex, impeded cell-cell adhesion and hindered intestinal barrier integrity. The increased *A. faecalis*-associated vinculin acetylation revealed that aberrant SCFAs derived from translocation of *A. faecalis* in colon tissues, could promote inflammation-to-cancer transition by modulating epithelial barrier integrity.

Despite the comprehensive insights gained, our study had several limitations. The focus on *A. faecalis*'s impact on Peyer's patches and colitis in a mouse model may not fully translate to human disease due to interspecies differences in immune responses and microbiota composition. Additionally, while we demonstrated significant changes in immune cell function and microbial composition, the precise molecular mechanisms remained to be elucidated. Further research should aim to identify specific bacterial metabolites or signaling pathways that mediate these effects, and longitudinal studies in human subjects could validate the relevance of our findings.

In conclusion, our study provided comprehensive understanding of how *A. faecalis* regulates intestinal immunity, influences intestinal barrier, to ultimately promote inflammation-to-cancer transition. By highlighting the dual role of *A. faecalis* in physiological and pathological conditions, we emphasized the importance of *A. faecalis*, opportunistic pathogens in Peyer's patches, in maintaining structural and immune homeostasis in inflammation-associated tumorigenesis. Our findings open new avenues for therapeutic intervention targeting *A. faecalis*-related microbial dysbiosis to prevent IBD-involved CRC.

Disclosure statement

No potential conflict of interest was reported by the author(s).

Funding

This project was supported by the National Natural Science Foundation of China, Project Number: 82274196, U22A20368, 82374233; the National Key Research and Development Program of China, Project Number: 2023YFC3502800, 2023YFC3502803; the Open Research Project of State Key Laboratory of Dampness Syndrome of Chinese Medicine, Project Number: SZ2022KF09; Incubation Program for the Science and Technology Development of Chinese Medicine Guangdong Laboratory, Project Number: HQL2024PZ040; the Talent Support Project of Guangdong, Project Number: 2021JC050230, National TCM inheritance and innovation project, Project Number: 2022QN13.

ORCID

Linlin Lu http://orcid.org/0000-0002-8221-4613

Acknowledgments

This Project was supported by the National Natural Science Foundation of China, Project Number: 82274196, U22A20368, 82374233; the National Key Research and Development Program of China, Project Number: 2023YFC3502800, 2023YFC3502803; the Open Research Project of State Key Laboratory of Dampness Syndrome of Chinese Medicine, Project Number: SZ2022KF09; Incubation Program for the Science and Technology Development of Chinese Medicine Guangdong Laboratory, Project Number: HQL2024PZ040; the Talent Support Project of Guangdong, Project Number: 2021JC050230, National TCM inheritance and innovation project, Project Number: 2022QN13. The authors thank BioRender.com for providing the tools to create scientific illustrations.

Abbreviations used in this study

IBD	Inflammatory bowel disease
CAC	Colitis-associated Cancer
CRC	Colorectal Cancer
A. faecalis	*Alcaligenes faecalis*
DSS	Dextran sulfate sodium salt
FAE	Follicle associated epithelium
SED	Sub-epithelial dome
IF	Interfollicular region
GC	Germinal center
DCs	Dendritic cells
GALTs	Gut-associated lymphoid tissues
ILFs	Isolated lymphoid follicles

MLNs	Mesenteric lymph nodes
ILP	Intestinal lamina propria.

Author contributions

Linlin Lu, Zhongqiu Liu, and Rong Zhang performed conceptualization, funding acquisition, project administration, supervision, writing and editing. Jing Zheng carried out data curation, validation, formal analysis, methodology, validation, resources, software and writing. Chishun Zhou and Zizheng Li participated data curation, methodology, validation. Xin Jin provided clinical resources. Yihua Zou, Shasha Bai, Huanjin Zheng, Weichao Ling, and Yiru Zhao participated methodology. Ying Wang supported resources.

Ethics statement

Clinical trials were conducted after obtaining informed consent from the patients in accordance with the management regulations and requirements of Guangzhou University of Chinese Medicine (Ethics number: K-2023-010).

All animal experiments were conducted in accordance with the Guangdong Provincial Laboratory Animal Management Guidelines and approved by the Animal Experiment Committee of the International Institute of Translational Medicine of Guangzhou University of Chinese Medicine (Permit number: SYXK(Guangdong)2019–0144).

References

1. Sender R, Fuchs S, Milo R. Revised estimates for the number of human and bacteria cells in the body. PLoS Biol. 2016;14(8):e1002533. doi:10.1371/journal.pbio.1002533.
2. Rebersek M. Gut microbiome and its role in colorectal cancer. BMC Cancer. 2021;21(1):1325. doi:10.1186/s12885-021-09054-2.
3. Wong CC, Yu J. Gut microbiota in colorectal cancer development and therapy. Nat Rev Clin Oncol. 2023;20(7):429–452. doi:10.1038/s41571-023-00766-x.
4. Haneishi Y, Furuya Y, Hasegawa M, Picarelli A, Rossi M, Miyamoto J. Inflammatory bowel diseases and gut microbiota. IJMS. 2023;24(4):24. doi:10.3390/ijms24043817.
5. Hou K, Wu ZX, Chen XY, Wang J-Q, Zhang D, Xiao C, Zhu D, Koya JB, Wei L, Li J, et al. Microbiota in health and diseases. Sig Transduct Target Ther. 2022;7(1):135. doi:10.1038/s41392-022-00974-4.
6. Zhao L, Zhang X, Zuo T, Yu J. The composition of colonic commensal bacteria according to anatomical localization in colorectal cancer. Engineering. 2017;3(1):90–97. doi:10.1016/J.ENG.2017.01.012.
7. Thaiss CA, Zmora N, Levy M, Elinav E. The microbiome and innate immunity. Nature. 2016;535(7610):65–74. doi:10.1038/nature18847.
8. Zheng D, Liwinski T, Elinav E. Interaction between microbiota and immunity in health and disease. Cell Res. 2020;30(6):492–506. doi:10.1038/s41422-020-0332-7.
9. Jung C, Hugot JP, Barreau F. Peyer's patches: the immune sensors of the intestine. Int J Inflammat. 2010;2010:1–12. doi:10.4061/2010/823710.
10. Obata T, Goto Y, Kunisawa J, Sato S, Sakamoto M, Setoyama H, Matsuki T, Nonaka K, Shibata N, Gohda M, et al. Indigenous opportunistic bacteria inhabit mammalian gut-associated lymphoid tissues and share a mucosal antibody-mediated symbiosis. Proc Natl Acad Sci USA. 2010;107(16):7419–7424. doi:10.1073/pnas.1001061107.
11. Wang Y, Hosomi K, Shimoyama A, Yoshii K, Nagatake T, Fujimoto Y, Kiyono H, Fukase K, Kunisawa J. Lipopolysaccharide derived from the lymphoid-resident commensal bacteria Alcaligenes faecalis functions as an effective nasal adjuvant to augment IgA antibody and Th17 cell responses. Front Immunol. 2021;12:699349. doi:10.3389/fimmu.2021.699349.
12. Hasan MJ, Nizhu LN, Rabbani R. Bloodstream infection with pandrug-resistant Alcaligenes faecalis treated with double-dose of tigecycline. IDCases. 2019;18:e00600. doi:10.1016/j.idcr.2019.e00600.
13. Takahashi K, Tsuji M, Nakagawasai O, Miyagawa K, Kurokawa K, Mochida-Saito A, Iwasa M, Iwasa H, Suzuki S, Takeda H, et al. Anxiolytic effects of enterococcus faecalis 2001 on a mouse model of colitis. Sci Rep. 2024;14(1):11519. doi:10.1038/s41598-024-62309-3.
14. Jans C, Boleij A. The road to infection: host-microbe interactions defining the pathogenicity of streptococcus bovis/streptococcus equinus complex members. Front Microbiol. 2018;9:603. doi:10.3389/fmicb.2018.00603.
15. Zhan Z, Tang H, Zhang Y, Huang X, Xu M. Potential of gut-derived short-chain fatty acids to control enteric pathogens. Front Microbiol. 2022;13:976406. doi:10.3389/fmicb.2022.976406.
16. Shimoyama A, Di Lorenzo F, Yamaura H, Mizote K, Palmigiano A, Pither MD, Speciale I, Uto T, Masui S, Sturiale L, et al. Lipopolysaccharide from gut-associated lymphoid-tissue-resident alcaligenes faecalis: complete structure determination and chemical synthesis of its lipid a. Angew Chem Int Ed Engl. 2021;60(18):10023–10031. doi:10.1002/anie.202012374.
17. Kunisawa J, Kiyono H. Alcaligenes is commensal bacteria habituating in the gut-associated lymphoid tissue for the regulation of intestinal IgA responses. Front Immun. 2012;3:65. doi:10.3389/fimmu.2012.00065.
18. Kobayashi N, Takahashi D, Takano S, Kimura S, Hase K. The roles of Peyer's patches and microfold cells in the gut immune system: relevance to

autoimmune diseases. Front Immunol. 2019;10:2345. doi:10.3389/fimmu.2019.02345.

19. Nagashima K, Sawa S, Nitta T, Tsutsumi M, Okamura T, Penninger JM, Nakashima T, Takayanagi H. Identification of subepithelial mesenchymal cells that induce IgA and diversify gut microbiota. Nat Immunol. 2017;18(6):675–682. doi:10.1038/ni.3732.
20. Macpherson AJ, Yilmaz B, Limenitakis JP, Ganal-Vonarburg SC. IgA function in relation to the intestinal microbiota. Annu Rev Immunol. 2018;36(1):359–381. doi:10.1146/annurev-immunol-042617-053238.
21. Zhang L, Shi X, Qiu H, Liu S, Yang T, Li X, Liu X. Protein modification by short-chain fatty acid metabolites in sepsis: a comprehensive review. Front Immunol. 2023;14:1171834. doi:10.3389/fimmu.2023.1171834.